

# Global Potential Energy Surface Investigation of Cyanoformaldehyde and Its Conformational Dynamics, Decomposition Pathways, and Water-Involved Bimolecular Reactions

Dapeng Zhang and Naoki Kishimoto\*

Cite This: *ACS Omega* 2025, 10, 18924–18935

Read Online

ACCESS |



Metrics &amp; More

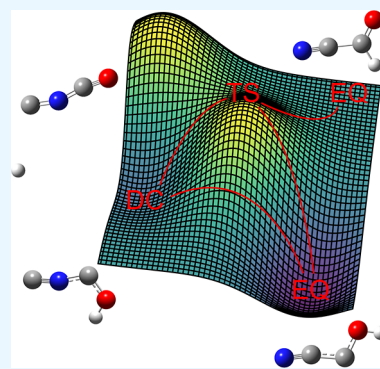


Article Recommendations



Supporting Information

**ABSTRACT:** Cyanoformaldehyde [HC(O)CN], a detected interstellar molecule, exhibits potential isomeric transformations that remain incompletely understood. Understanding its conformational flexibility is crucial for predicting its reactivity in interstellar conditions. This study presents a comprehensive investigation of the complete HC(O)CN potential energy surface (PES) using the anharmonic downward distortion following (ADDF) algorithm, enabling exhaustive mapping of EQs, TSs, DCs, and connecting pathways. At the B3LYP-D3(BJ)/def2-TZVP level of theory, our analysis reveals 48 EQs, 152 TSs, and 49 DCs. We identify 80 unique isomerization pathways mediated by TS structures (EQ<sub>x</sub>–TS<sub>n</sub>–EQ<sub>y</sub>), complemented by 34 TS-mediated (EQ<sub>a</sub>–TS<sub>b</sub>–DC) and 40 direct (EQ<sub>m</sub>–DC<sub>n</sub>) DCs. The multicomponent artificial force induced reaction (MC-AFIR) method is employed to generate stochastic conformational ensembles comprising the most stable isomers in investigations and a single water molecule, enabling systematic analysis of product formation propensities. These findings provide a comprehensive database of conformational relationships, thermodynamic behaviors, and water-involved reactions for HC(O)CN isomers. Our analysis establishes a reference framework for predicting isomer stability, interconversion pathways, and reactivity under various conditions.



## INTRODUCTION

The investigation of a potential energy surface (PES) provides critical insights into the electronic and structural properties of stable isomers, enabling the quantification of their conformational parameters, relative energies, and the potential reaction pathways interlinking them. Although conventional principles suggest that the formation propensities of isomers should correlate with relative stabilities, extensive astrochemical observations reveal that the detection of isomers in the interstellar medium (ISM) is governed by a complex interplay of factors beyond thermodynamic considerations alone, making higher-energy species potentially observable.<sup>1–6</sup> Given the importance of lowest-energy and higher-energy isomers, systematic and global investigation of their PES is essential for identifying potential isomeric structures and understanding the fundamental mechanisms that govern their molecular evolution, including conformational isomerization, dissociative processes yielding smaller molecular fragments, and subsequent reactions leading to the formation of more complex molecular assemblies.<sup>7</sup>

Cyanoformaldehyde [HC(O)CN or HCOCN], also known as formyl cyanide, readily hydrolyze to yield formic acid and hydrogen cyanide.<sup>8</sup> This molecule has been extensively characterized through spectroscopic studies<sup>9–11</sup> and subsequently detected in the Sgr B2(N) molecular cloud using the

Green Bank Telescope by Remijan et al.<sup>12</sup> Gronowski et al. conducted theoretical investigations into the structural properties of stable isomers of HC(O)CN, providing detailed spectroscopic parameters.<sup>13</sup> Several studies have extensively examined its molecular behavior, particularly focusing on potential formation mechanisms, transformation processes, and dissociation pathways.<sup>14–17</sup> Additionally, theoretical investigations have characterized its reactivity with various small molecules (HNO, HF, HCl, H<sub>2</sub>O, and CH<sub>3</sub>OH).<sup>18</sup> Despite extensive research on the chemical properties of HC(O)CN, a global investigation of its PES focusing on conformational isomerism and associated interconversion pathways remains unexplored in the report.

The scaled hypersphere search with anharmonic downward distortions following (SHS-ADDF) method facilitates automated and efficient investigation of PES, independent of molecular size.<sup>19,20</sup> The approach employs systematically scaled hyperspheres centered at each PES minimum to identify

Received: January 31, 2025

Revised: April 23, 2025

Accepted: April 25, 2025

Published: April 28, 2025



critical points. The algorithm proceeds in two phases: first, it traces uphill pathways from minima to locate transition state structures (TSs) and dissociation channels (DCs), then calculates intrinsic reaction coordinates (IRC) bidirectionally from each TS to identify connected equilibrium (EQ) structures or DCs. Through iterative implementation, this methodology enables the construction of comprehensive reaction networks.<sup>21–25</sup> In the present investigation, we apply the SHS-ADDF algorithm to explore the chemical space of HC(O)CN, identifying its EQ, TS, and DC structures, and the associated isomerization pathways and dissociation mechanisms.

In this paper, to investigate the bimolecular reaction of HC(O)CN, its reactivity with H<sub>2</sub>O molecules is systematically studied through quantum chemical calculations. While conformational analysis using the SHS-ADDF method effectively explores single-component systems, it has inherent limitations in characterizing intermolecular reactions. Herein, we employ multicomponent artificial force induced reaction (MC-AFIR) approach,<sup>26–28</sup> which provides a robust framework for examining bimolecular reactions. We have systematically studied the potential reactions between a single H<sub>2</sub>O molecule and the most stable isomers identified from our conformational investigation by applying artificial forces between the dimeric fragments. For each artificial force, multiple trials are performed to ensure statistical significance. The product formation probability is calculated as the ratio of specific products to the total number of EQ structures from all AFIR pathways. This comprehensive investigation of HC(O)CN includes both a thorough PES investigation revealing complete reaction route maps and a systematic study of its bimolecular reactions with H<sub>2</sub>O. The precise characterization of isomerization mechanisms and dissociation pathways provides fundamental insights into HC(O)CN reactivity, offering valuable reference for understanding similar molecular systems and potentially contributing to our knowledge of conformational and thermodynamical processes.

## COMPUTATIONAL DETAILS

The PES of cyanoformaldehyde is fully investigated using the global reaction route mapping (GRRM) program (version 17)<sup>29,30</sup> in conjunction with Gaussian 16.<sup>31</sup> The GRRM program's core function, the anharmonic downward distortion following (ADDF) algorithm,<sup>19,20,22,23,32</sup> systematically explores the PES from an initial EQ structure to locate stable minima. The extent of investigation is determined by the specified size of anharmonic downward distortions (ADDs) between harmonic and real potentials on the PES. The ADDF search protocol can be constrained for complicated and flexible systems or executed without constraints to fully map stable minima and DCs, thereby enabling automated and efficient identification of isomerization pathways and DCs. During this process, TSs are identified simultaneously, with DCs comprising direct and TS-mediated pathways.

The ADDF calculation provides lists of EQ, TS, and DC in the explored sequence. For the EQ list, from EQ<sub>0</sub> to EQ<sub>*x*</sub>; for the TS list, from TS<sub>0</sub> to TS<sub>*n*</sub>, as well as the connection of each TS. When a TS connects two distinct EQs, a pathway of EQ<sub>*x*</sub>–TS<sub>*n*</sub>–EQ<sub>*y*</sub> can be established; when a TS connects an EQ and a DC, a path of EQ<sub>*a*</sub>–TS<sub>*b*</sub>–DC can be identified; for the DC list, from DC<sub>0</sub> to DC<sub>*n*</sub>, an EQ<sub>*m*</sub>–DC<sub>*n*</sub> pathway can be determined. For clarity, the notations *x*, *y*, *m*, *n*, *a*, and *b* are employed. Notably, only verified TSs and DCs are mapped in

the final isomerization network, resulting in a subset of the initially explored structures. Several types of identified isomers are excluded from the final maps: (1) initially identified TS<sub>*n*</sub>/*n* structures that reverted to their corresponding EQ<sub>*n*</sub> configurations upon optimization, and thus do not represent true TSs; (2) TSs connecting to unidentified EQs; (3) TSs connecting two DCs; and (4) TSs that do not yield thermodynamically reasonable pathways.

The initial HC(O)CN structure is optimized at the B3LYP-D3(BJ)/def2-TZVP level of theory,<sup>33–36</sup> which is subsequently employed for the ADDF calculations. Zero-point vibrational energies (ZPVE) corrections are incorporated into the global reaction route map. Final energies are refined using single-point-energy calculations with multiple high-level theoretical methods to validate the accuracy of the explored structures (Figures S1–S4). The comparative analysis employ the range-separated hybrid functional ωB97X-D with def2-QZVPP basis set,<sup>35–37</sup> followed by calculations using the range-separated double-hybrid functional RSX-PBE-QIDH with def2-QZVPP basis set.<sup>35,36,38,39</sup> Further refinements include second-order Møller–Plesset perturbation theory (MP2) with aug-cc-pVTZ basis set,<sup>40–42</sup> and coupled-cluster theory with single, double, and perturbative triple excitations [CCSD(T)] with aug-cc-pVTZ basis set.<sup>41–43</sup>

The five most stable isomers are selected for reactive studies with water molecules using the multicomponent artificial force induced reaction (MC-AFIR) method implemented in the GRRM program. This method facilitates structural deformations by driving fragments together or preventing their proximity, as defined by the following equation.<sup>26</sup>

$$F_{\text{AFIR}}(\mathbf{Q}) = E(\mathbf{Q}) + \rho\alpha \times \left\{ \sum_{i \in A} \sum_{j \in B} \left( \frac{R_i + R_j}{r_{ij}} \right)^6 r_{ij} \right\} / \left\{ \sum_{i \in A} \sum_{j \in B} \left( \frac{R_i + R_j}{r_{ij}} \right)^6 \right\}$$

The PES  $E(\mathbf{Q})$  is defined by geometrical parameters  $\mathbf{Q}$ , where  $\alpha$  represents the force parameter and  $\rho$  is assigned a value of either 1.0 or –1.0. The weighted term comprises the summation of interatomic distance  $r_{ij}$  between atoms  $i$  and  $j$ , with  $R_i$  and  $R_j$  denoting the respective covalent radii of these atoms. The force constant,  $\alpha$ , is expressed through the following equation.<sup>26</sup>

$$\alpha = \frac{\gamma}{\left\{ 2^{\frac{-1}{6}} - \left( 1 + \sqrt{1 + \frac{\gamma}{\varepsilon}} \right)^{\frac{-1}{6}} \right\} R_0}$$

The parameters  $R_0$  and  $\varepsilon$  are equivalent to the Lennard–Jones potential from Ar–Ar interactions (3.8164 Å and 1.0061 kJ/mol, respectively). The parameter  $\alpha$  represents the mean force experienced by an Ar–Ar pair during its trajectory from the energy minimum to the collision turning point during a direct interaction with energy  $\gamma$ . The collision energy parameter  $\gamma$ , which is manually defined in calculations, determines the barrier height that can be overcome using the AFIR calculations.<sup>26</sup>

During calculation, initial structures are automatically generated by random orientations and positions of the fragments. For each initial structure, the algorithm computes different AFIR paths (trajectories during the minimization of

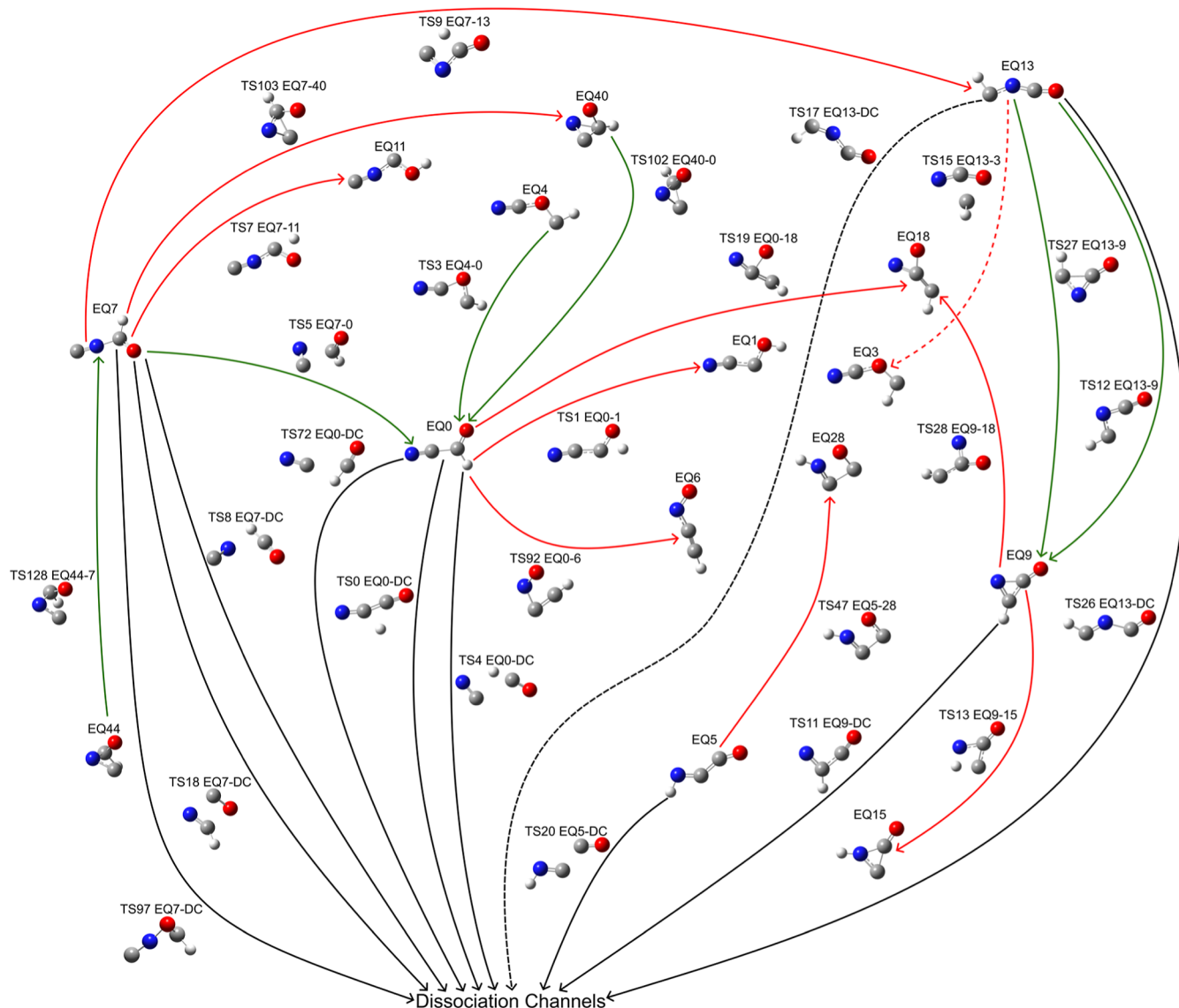


**Figure 1.** Reaction route map of isomerization pathways and TS-mediated dissociation channels (DCs) for EQ0, EQ5, EQ7, EQ9, and EQ13. The reaction network illustrates isomerization pathways and DCs. Red arrows denote conformational changes from more stable structures to less stable isomers, green arrows depict transitions toward more stable isomers and black arrows indicate pathways leading to DCs with TS barriers. Dashed lines denote pathways equivalent in significance to those depicted by solid lines.

the AFIR function) while maintaining the identity of fragments. Along each AFIR path, local minima and maxima are identified, which correspond to approximate EQs and TSs on the potential energy surface  $E(\mathbf{Q})$ , respectively. In this study, artificial forces are applied between HC(O)CN and H<sub>2</sub>O molecules to induce reactions, with both reactants treated as separate fragments randomly distributed during structure generation. The initial parameter  $\gamma$  is initialized with stochastic values of 100s, 200s, and 400s kJ/mol, where  $s$  denotes a random number between 0 and 1. During the AFIR path search,  $\gamma$  is systematically increased to reach values of 100, 200, and 400 kJ/mol, respectively. The MC-AFIR calculations are terminated upon reaching 50 AFIR paths (NSample = 50) or when 10 consecutive AFIR paths fail to identify new products (NFault = 10). Each MC-AFIR calculation with the same  $\gamma$  value is repeated in triplicate for each EQ structure. The MC-AFIR calculations are performed at the B3LYP-D3(BJ)/def2-TZVP level of theory.

## RESULTS AND DISCUSSION

Through systematic conformational analysis of an optimized HC(O)CN molecule, we identify 48 EQs, 152 TSs, and 49 DCs that proceed without traversing a TS structure. The global reaction route network (see the global reaction map in the Supporting Information) consists of 80 isomerization processes that connect EQs through TSs and the TS-mediated DCs. The ZPVE-corrected relative energies at 0 K for full paths are detailed in Table S1. The stability of HC(O)CN and its isomers under interstellar conditions is assessed by comparing calculated energy barriers with typical interstellar UV radiation energies (138.4–313.6 kcal/mol).<sup>44</sup> Our analysis indicates that most isomerization pathways have barriers below this energy range, suggesting that these species may require shielded environments to maintain detectable abundances in the ISM. Figure 1 shows the isomerization pathways (see also the relative energies shown in Figure S5) and TS-mediated dissociations relevant to the five most stable isomers identified

in ADDF calculation. These include the global minimum structure (EQ0) and four higher-energy isomers (EQ7, EQ9, EQ5, and EQ13), with relative free energies of 0, 11.1, 28.9, 31.8, and 42.9 kcal/mol at 298.15 K, respectively. These isomers remain thermodynamically stable across a range of temperatures, with EQ0 being the most predominant species (Table S2). Notably, the current study focuses on the investigation of the PES, where the formation propensity of each isomer can be estimated through thermodynamical considerations. However, dynamical aspects, especially at low-temperature conditions, are not included in this analysis. Further investigations regarding the investigated isomerization pathways would be necessary to understand the reaction kinetics. Table 1 summarizes the relative energies associated

**Table 1. Relative ZPVE-Corrected Energies of Isomerization Pathways at 0 K (kcal/mol)**

pathways	EQ <sub>x</sub>	TS <sub>m</sub> <i>x</i> – <i>y</i>	energy barrier	EQ <sub>y</sub>
EQ0-TS1-EQ1	0	79.1	79.1	45.8
EQ4-TS3-EQ0	86.8	104.0	17.2	0
EQ7-TS5-EQ0	11.2	42.6	31.4	0
EQ7-TS7-EQ11	11.2	88.3	77.1	54.6
EQ7-TS9-EQ13	11.2	73.8	62.6	42.6
EQ13-TS12-EQ9	42.6	53.1	10.5	28.5
EQ9-TS13-EQ15	28.5	98.4	69.9	71.4
EQ13-TS15-EQ3	42.6	111.2	68.6	81.0
EQ0-TS19-EQ18	0	146.5	146.5	143.2
EQ13-TS27-EQ9	42.6	74.1	31.5	28.5
EQ9-TS28-EQ18	28.5	149.8	121.3	143.2
EQ5-TS47-EQ28	31.5	163.9	132.4	163.7
EQ0-TS92-EQ6	0	151.9	151.9	81.0
EQ40-TS102-EQ0	141.0	144.6	3.6	0
EQ7-TS103-EQ40	11.2	157.9	146.7	141.0
EQ44-TS128-EQ7	165.6	167.4	1.8	11.2

with these isomerization pathways. Additional pathways are detailed in the Supporting Information. The geometrical parameters of these structures are compared with those from further optimization at the CCSD(T)/aug-cc-pVTZ level of

theory, confirming the reliability and accuracy of the ADDF calculations (Table S3).

EQ0 is a structure of HC(O)CN, while EQ7 is a structure of HC(O)NC in which the carbon atom bonded to the –C(O)H group exchanges position with the nitrogen atom. Via the pathway EQ7-TS5-EQ0, the HC(O)NC to HC(O)CN isomerization involves the rearrangement of the isocyano group (–NC) into a cyano group (–CN) with an energy barrier of 31.4 kcal/mol, which is notably lower than the barriers required for transformations to thermodynamically less stable isomers. Hydrogen atom migration occurs via the EQ0-TS1-EQ1 pathway, where the hydrogen within the aldehyde group [HC(O)–] ultimately forms a hydroxy group (HOC–), overcoming a high energy barrier of 79.1 kcal/mol. Oxygen migration is observed through the EQ0-TS19-EQ18 pathway, in which an oxygen atom shifts from the HC(O)– group and bonds to a different carbon atom, yielding the HCC(O)N isomer with a significant barrier of 146.5 kcal/mol. Additionally, the EQ0-TS92-EQ6 pathway facilitates the isomerization of HC(O)CN to HCCNO via oxygen translocation from the carbon to the terminal nitrogen atom, surmounting a substantial energy barrier of 151.9 kcal/mol. These high energy barriers illustrate the thermodynamic control over potential isomerization pathways of HC(O)CN, with transformations to higher-energy isomers generally requiring substantially higher activation energies.

A similar hydrogen migration occurs via the EQ7-TS7-EQ11 pathway, where the hydrogen atom in the HC(O)– group forms an HOC– group, requiring a high energy barrier of 77.1 kcal/mol. A large energy barrier of 62.5 kcal/mol is also observed in the EQ7-TS9-EQ13 pathway, where hydrogen migrates from HC(O)– to –NCH to form a linear OCNCH isomer. In the EQ9-TS13-EQ15 pathway, the hydrogen atom migrates from a carbon atom to bond with the nitrogen atom within the ring, creating an O–c-CCN–H structure with an energy barrier of 69.9 kcal/mol. Complex rearrangements among HC(O)CN isomers involve various structural transformations. In the EQ4-TS3-EQ0 pathway, the HCO– moiety bonded to the –CN moiety reorganizes to form a HC(O)– group, facilitating the isomerization of HOCCN to HC(O)CN with an energy barrier of 17.2 kcal/mol. This

**Table 2. Relative Energies of TS-Mediated DCs at 0 K (kcal/mol)**

pathways	explored EQ <sub>a</sub>	explored TS <sub>b</sub> <i>a</i> -DC	dissociation energy	pathways	explored EQ <sub>a</sub>	explored TS <sub>b</sub> <i>a</i> -DC	dissociation energy
EQ0-TS0-DC	0	71.8	71.8	EQ25-TS57-DC	75.1	135.5	60.4
EQ0-TS4-DC	0	61.3	61.3	EQ26-TS58-DC	146.7	173.2	26.5
EQ7-TS8-DC	11.2	61.8	50.6	EQ3-TS61-DC	81.0	136.7	55.7
EQ9-TS11-DC	28.5	40.5	12.0	EQ4-TS63-DC	86.8	107.0	20.2
EQ16-TS14-DC	118.8	127.8	9.0	EQ12-TS64-DC	56.9	93.0	36.1
EQ13-TS17-DC	42.6	49.4	6.8	EQ35-TS69-DC	105.1	178.0	72.9
EQ7-TS18-DC	11.2	94.3	83.1	EQ0-TS72-DC	0	62.1	62.1
EQ5-TS20-DC	31.5	34.5	3.0	EQ16-TS87-DC	118.8	127.2	8.4
EQ20-TS22-DC	161.5	198.2	36.7	EQ39-TS95-DC	127.9	128.2	0.3
EQ13-TS26-DC	42.6	51.8	9.2	EQ39-TS96-DC	127.9	159.5	31.6
EQ2-TS34-DC	49.2	92.0	42.8	EQ7-TS97-DC	11.2	162.9	151.7
EQ12-TS40-DC	56.9	88.2	31.3	EQ31-TS125-DC	162.2	206.3	44.1
EQ15-TS43-DC	71.4	102.9	31.5	EQ20-TS127-DC	161.5	246.0	84.5
EQ26-TS45-DC	146.7	160.5	13.8	EQ44-TS130-DC	165.6	177.2	11.6
EQ27-TS46-DC	98.5	104.7	6.2	EQ44-TS131-DC	165.6	177.6	12.0
EQ29-TS48-DC	119.3	172.3	53.0	EQ44-TS132-DC	165.6	190.8	25.2
EQ25-TS55-DC	75.1	76.4	1.3	EQ26-TS141-DC	146.7	184.6	37.9

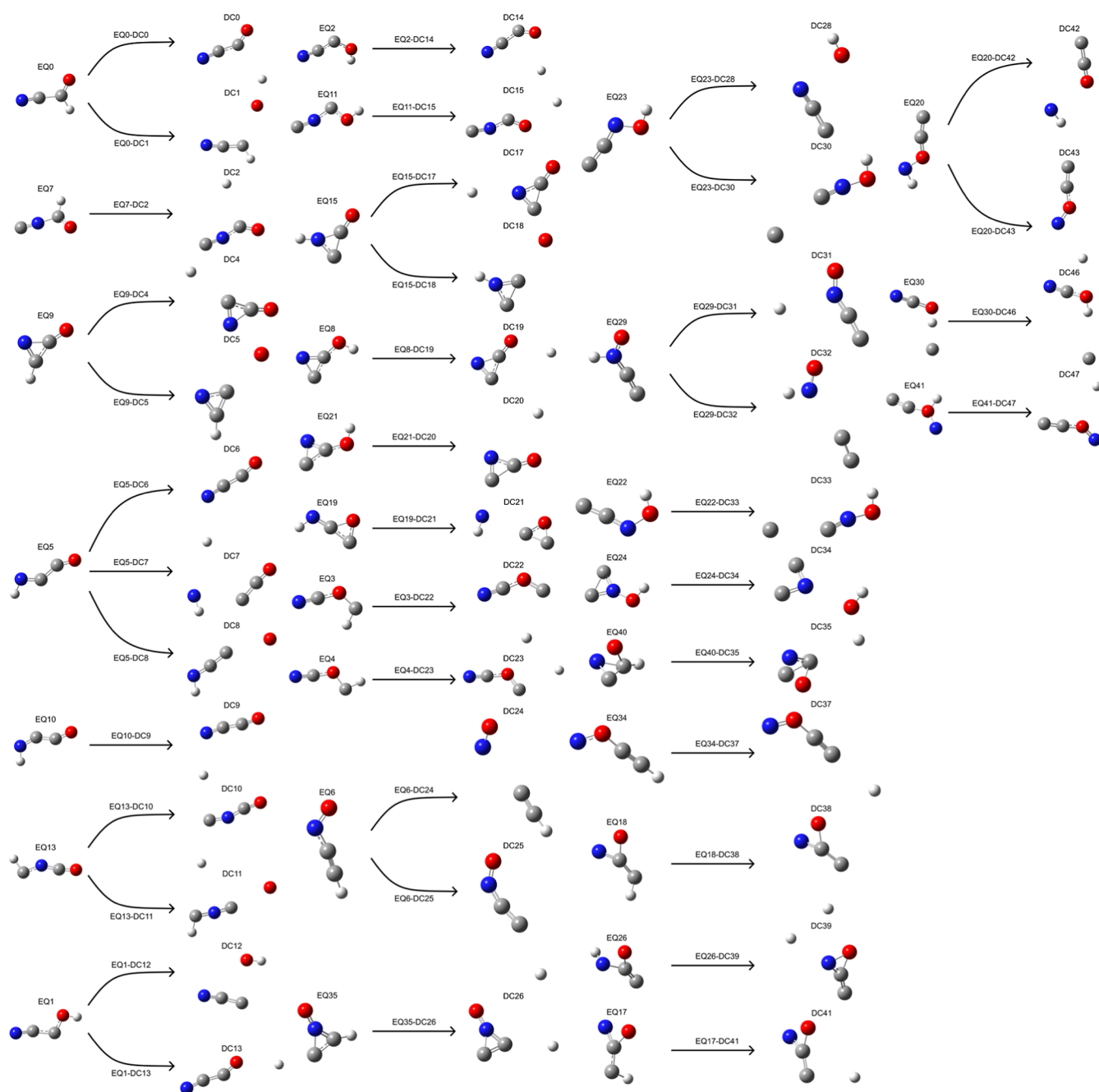


**Figure 2.** Direct DCs for cyanoformaldehyde. The notation  $EQ_m$ - $DC_n$  indicates the pathway from  $EQ_m$  to  $DC_n$ .

suggests a thermodynamically favorable route back to the global minimum structure, consistent with the tendency of chemical systems to evolve toward their most stable configurations. In the  $EQ_{13}$ - $TS_{15}$ - $EQ_3$  pathway, the  $-CH$  and  $-OCN-$  moieties of linear  $OCNCH$  undergo rearrangement to form  $HCOCN$ , necessitating a high energy barrier of 68.6 kcal/mol.

We identify isomerization pathways associated with cyclization among distinct isomers. The transformation of  $HC(O)NC$  to  $H-c-C(O)CN$  proceeds via the  $EQ_7$ - $TS_{103}$ - $EQ_{40}$  pathway, requiring a substantial energy barrier of 146.7 kcal/mol. Cyclization of the  $-CNC-$  moiety occurs through the  $EQ_{13}$ - $TS_{12}$ - $EQ_9$  and  $EQ_{13}$ - $TS_{27}$ - $EQ_9$  pathways, yielding the cyclic  $O-c-CNC-H$  structure with energy barriers of 10.5 and 31.5 kcal/mol, respectively. This

difference in energy barriers can be attributed to the cyclic structure of  $TS_{27}$ , which introduces additional strain compared to the more flexible structure  $TS_{12}$ . The  $EQ_9$ - $TS_{28}$ - $EQ_{18}$  pathway features a ring-opening of the  $O-c-CNC-H$  structure followed by molecular rearrangement, leading to the formation of the  $HCC(O)N$  isomer with a pronounced energy requirement of 121.3 kcal/mol. Additionally, the  $EQ_5$ - $TS_{47}$ - $EQ_{28}$  pathway denotes the cyclization of the linear  $HNCCO$  isomer, requiring a significant energy barrier of 132.4 kcal/mol. Hydrogen and oxygen atom migrations also occur in cyclic structures, facilitating the conversion of the  $H-c-C(O)CN$  isomer to  $HC(O)NC$  via the  $EQ_{44}$ - $TS_{128}$ - $EQ_7$  pathway, with a negligible energy barrier of 1.8 kcal/mol. The  $H-c-C(O)CN$  structure can undergo a ring opening process to form  $HC(O)NC$  via

Table 3. Relative Energies of Direct DCs at 0 K (kcal/mol)

pathways	explored EQ <sub>m</sub>	DC <sub>n</sub>	dissociation energy	pathways	explored EQ <sub>m</sub>	DC <sub>n</sub>	dissociation energy
EQ0–DC0	0	104.4	104.4	EQ3–DC22	81.0	180.4	99.4
EQ0–DC1	0	218.4	218.4	EQ4–DC23	86.8	180.9	94.1
EQ7–DC2	11.2	124.0	112.8	EQ6–DC24	81.0	149.5	68.5
EQ9–DC4	28.5	136.7	108.2	EQ6–DC25	81.0	215.6	134.6
EQ9–DC5	28.5	215.9	187.4	EQ35–DC26	105.1	221.5	116.4
EQ5–DC6	31.5	122.4	90.9	EQ23–DC28	118.0	185.0	67.0
EQ5–DC7	31.5	220.9	189.4	EQ23–DC30	118.0	249.8	131.8
EQ5–DC8	31.5	247.0	215.5	EQ29–DC31	119.3	210.3	91.0
EQ10–DC9	47.2	120.2	73.0	EQ29–DC32	119.3	226.7	107.4
EQ13–DC10	42.6	133.4	90.8	EQ22–DC33	119.1	249.6	130.5
EQ13–DC11	42.6	236.3	193.7	EQ24–DC34	139.6	194.0	54.4
EQ1–DC12	45.8	171.8	126.0	EQ40–DC35	141.0	272.2	131.2
EQ1–DC13	45.8	124.7	78.9	EQ34–DC37	141.3	283.6	142.3
EQ2–DC14	49.2	119.3	70.1	EQ18–DC38	143.2	252.4	109.2
EQ11–DC15	54.6	142.0	87.4	EQ26–DC39	146.7	254.7	108.0
EQ15–DC17	71.4	143.8	72.4	EQ17–DC41	156.1	248.4	92.3
EQ15–DC18	71.4	249.7	178.3	EQ20–DC42	161.5	227.5	66.0
EQ8–DC19	62.2	147.4	85.2	EQ20–DC43	161.5	274.0	112.5
EQ21–DC20	70.8	147.2	76.4	EQ30–DC46	184.7	189.9	5.2
EQ19–DC21	86.4	242.3	155.9	EQ41–DC47	241.1	287.1	46.0

EQ40–TS102–EQ0, accompanied by a negligible barrier of 3.6 kcal/mol. Although these pathways exhibit remarkably low energy barriers, the thermodynamic instability of EQ44 and EQ40 suggests these species may exist in extremely low formation propensities, limiting the practical significance of these isomerization pathways.

Analysis of the global reaction route map reveals 34 distinct TS-mediated DCs, which are thoroughly characterized and summarized in Table 2. The dissociation pathways of EQ0 proceed through two primary pathways. The EQ0–TS0–DC pathway leads to HC(O)CN fragmentation, yielding C(O)CN + H, while the EQ0–TS4–DC and EQ0–TS72–DC pathways result in HCO + CN fragmentation. Examining the reaction rate (Table S4) provides fundamental insights into the competition between dissociation and isomerization pathways. For the global minimum structure EQ0, the dissociation channels (particularly EQ0–TS4–DC) demonstrate significantly higher rate constants ( $5.1 \times 10^{-32} \text{ s}^{-1}$ ) compared to the isomerization pathway via EQ0–TS1–EQ1 ( $3.4 \times 10^{-45} \text{ s}^{-1}$ ). This pronounced kinetic preference suggests that under thermal conditions, HC(O)CN would predominantly undergo fragmentation to HCO + CN rather than isomerization.

For the HOCNC structure, dissociation occurs between carbon atoms via EQ2–TS34–DC. The HCOCN isomer exhibits two distinct fragmentation pathways: hydrogen atom dissociation (EQ3–TS61–DC) and HCO + CN fragmentation (EQ4–TS63–DC). Linear isomers demonstrate various TS-mediated dissociation mechanisms. The HNCCO isomer undergoes HNC + CO fragmentation (EQ5–TS20–DC), while kinetic analysis suggests that the dissociation pathway is more favorable than the isomerization pathway (EQ5–TS47–EQ28). HC(O)NC exhibits multiple pathways: CN + HCO fragmentation (EQ7–TS8–DC), HCN + CO fragmentation (EQ7–TS18–DC), and dissociation through a linear HCONC TS structure (EQ7–TS97–DC). For EQ7, analysis of the reaction rate constants reveals a preference for isomerization over dissociation pathways. The EQ7–TS5–EQ0 isomerization pathway exhibits a significantly higher rate constant ( $6.3 \times 10^{-11} \text{ s}^{-1}$ ) compared to the dissociation

channel EQ7–TS18–DC ( $6.2 \times 10^{-49} \text{ s}^{-1}$ ), indicating HC(O)NC preferentially converts to HC(O)CN rather than fragmenting under thermal conditions.

The HOCNC isomer fragments form CN + H + CO through two pathways (EQ12–TS40–DC and EQ12–TS64–DC). Cyclic structures display unique TS-mediated dissociation behaviors. The O–*c*-CNC–H structure undergoes ring-opening between nitrogen and carbon atoms (EQ9–TS11–DC), while O–*c*-CCN–H dissociates through ring-opening between carbon atoms (EQ15–TS43–DC). For EQ9, kinetic analysis reveals a substantial difference in reaction rates, with the dissociation pathway proceeding at  $1.6 \times 10^4 \text{ s}^{-1}$ , in stark contrast to an extremely low isomerization rate of  $1.9 \times 10^{-76} \text{ s}^{-1}$ . The H–*c*-CCON structure dissociates through rotational isomerization via two pathways (EQ16–TS14–DC and EQ16–TS87–DC). HN–*c*-COC demonstrates ring-opening to form either linear HNCCO (EQ25–TS55–DC) or HNCOC (EQ25–TS57–DC) structures.

Several isomers exhibit rotational isomerization during TS-mediated dissociation. EQ13 shows two dissociation pathways with rotational isomerization (EQ13–TS17–DC and EQ13–TS26–DC). For EQ13, both isomerization pathways and dissociation processes are kinetically feasible, with rate constants ranging from  $10^5$  to  $10^7 \text{ s}^{-1}$ . However, the isomerization routes vary depending on the TS structure: EQ13–TS12–EQ9 proceeds at a rate of  $1.5 \times 10^5 \text{ s}^{-1}$ , while EQ13–TS15–EQ3 exhibits a low-rate constant of  $4.1 \times 10^{-38} \text{ s}^{-1}$ . The linear HNOCC structure dissociates through a rotated TS (EQ20–TS22–DC) or forms NH + *c*-CCO fragments (EQ20–TS127–DC). HNC(O)C undergoes NH + CCO fragmentation (EQ26–TS45–DC) or dissociates through rotational isomerization forming cyclic H–*c*-NCCO TSs (EQ26–TS58–DC and EQ26–TS141–DC). Additional significant pathways include the H–*c*-NCOC isomer dissociating to HNC + CO (EQ27–TS46–DC) and ON(H)CC dissociating through a rotated TS (EQ29–TS48–DC). The HNOCC structure undergoes H + NOCC fragmentation (EQ31–TS125–DC), while H–*c*-CCN–O dissociates through ring-opening to form an HCN(O)C TS (EQ35–

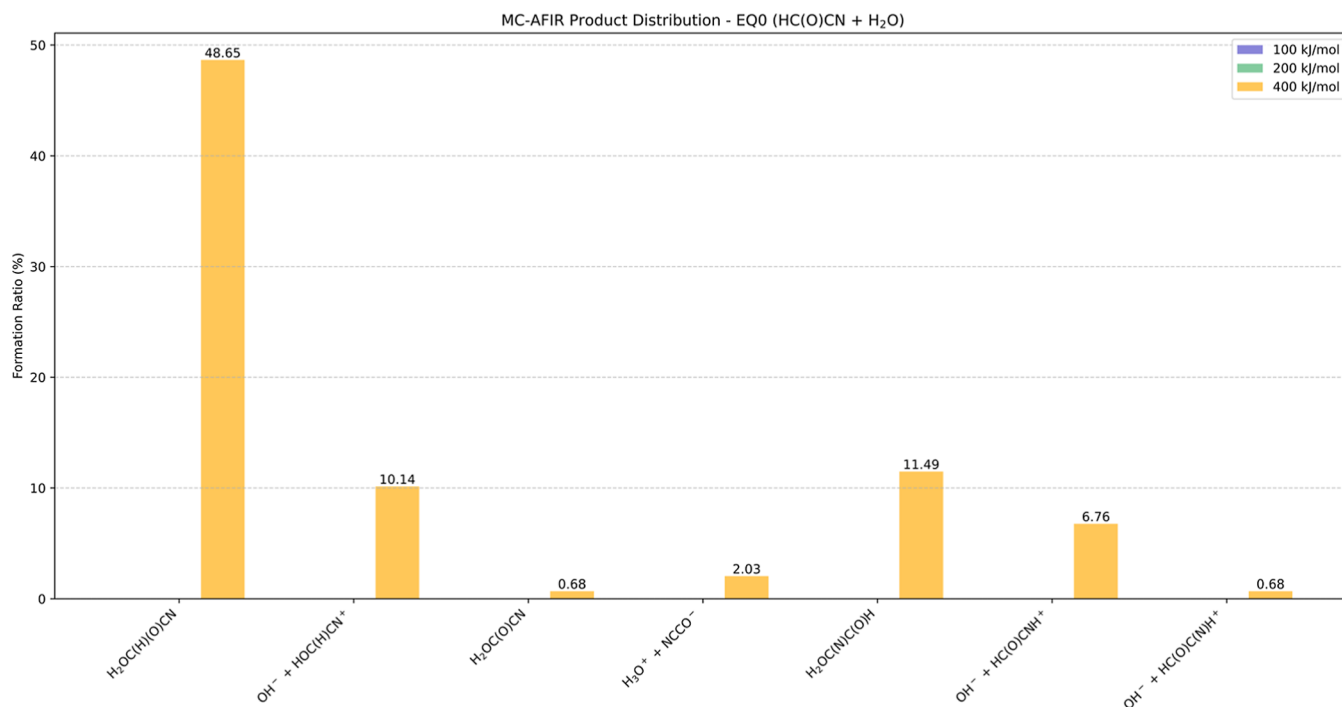


**Figure 3.** Predicted product distributions from MC-AFIR calculation for the reaction of HC(O)CN + H<sub>2</sub>O, starting from EQ0.

TS69–DC). The HCONC isomer exhibits two pathways: CN + HCO fragmentation (EQ39–TS95–DC) and rotational dissociation (EQ39–TS96–DC). Additionally, the H-*c*-C(O)CN structure shows multiple pathways, including formation of linear HCNC O TSs (EQ44–TS130–DC and EQ44–TS131–DC), and CO + HCN fragmentation (EQ44–TS132–DC).

The conformational investigation identifies 40 direct DCs, illustrated in Figure 2 and detailed in Table 3. These pathways are categorized based on their structural features and dissociation patterns. In ADDF calculation, a DC structure is identified when the atomic distance exceeds the threshold of  $2 \times (R^A + R^B)$ , where  $R^A$  and  $R^B$  are the covalent radii of atoms A and B. For the primary HC(O)CN conformer (EQ0), two DCs are identified: hydrogen atom dissociation (EQ0–DC0 pathway) and oxygen atom dissociation (EQ0–DC1 pathway). Similarly, the HC(O)NC isomer (EQ7) exhibits analogous dissociation pathways through hydrogen atom elimination via the EQ7–DC2 pathway. The cyclic and linear isomers demonstrate diverse fragmentation patterns. The O-*c*-CNC–H isomer undergoes hydrogen atom (EQ9–DC4 pathway) and oxygen atom (EQ9–DC5 pathway) dissociation. The linear HNCCO isomer exhibits three distinct pathways: hydrogen atom dissociation (EQ5–DC6 pathway), HN + CCO fragmentation (EQ5–DC7 pathway), and oxygen atom elimination (EQ5–DC8 pathway). OCCNH and OCNCH isomers undergo hydrogen atom dissociation (EQ10–DC9 and EQ13–DC10 pathways, respectively), with OCNCH additionally showing oxygen atom elimination (EQ13–DC11 pathway). The HOCNC isomer exhibits multiple pathways, including CCN + OH fragmentation (EQ1–DC12 pathway) and hydrogen atom dissociation (EQ1–DC13 and EQ2–DC14 pathways). The HOCNC system demonstrates hydrogen atom elimination (EQ11–DC15). The O-*c*-CCN–H structure shows both hydrogen (EQ15–DC17) and oxygen atom (EQ15–DC18) dissociation pathways, while cyclic HO–

*c*-CCN exhibits hydrogen atom dissociation through two distinct routes (EQ8–DC19, EQ21–DC20).

Complex fragmentation patterns are observed in several pathways. The HN-*c*-COC isomer dissociates to form HN + *c*-COC fragments (EQ19–DC21). HCCNO demonstrates NO + CCH fragmentation (EQ6–DC24) and hydrogen atom dissociation (EQ6–DC25). The HONCC isomer exhibits multiple pathways, including CCN + OH formation (EQ23–DC28) and terminal carbon dissociation yielding CNOH (EQ23–DC30). The ON(H)CC isomer shows both hydrogen atom dissociation (EQ29–DC31) and CC + ONH fragmentation (EQ29–DC32). The HCCON structure exhibits hydrogen atom (EQ34–DC37) dissociation pathways. The linear HNOCC structure demonstrates two distinct pathways: HN + CCO fragmentation (EQ20–DC42) and hydrogen atom dissociation (EQ20–DC43). The HCOCN isomer shows two distinct hydrogen atom DCs (EQ3–DC22 and EQ4–DC23 pathways). The cyclic H-*c*-CCN–O structure undergoes hydrogen atom (EQ35–DC26) elimination. The HONCC isomer demonstrates terminal carbon atom dissociation forming CNOH (EQ22–DC33), while the cyclic HO-*c*-NCC structure shows OH fragment elimination (EQ24–DC34). The cyclic H-*c*-C(O)CN isomer undergoes hydrogen atom dissociation (EQ40–DC35), while HCC(O)N exhibits two distinct hydrogen atom elimination pathways (EQ18–DC38, EQ17–DC41). The HNC(O)C structure shows concurrent hydrogen atom dissociation and terminal carbon atom elimination, forming H-*c*-NCO (EQ26–DC39 pathway). The cyclic HO-*c*-CCN demonstrates carbon atom dissociation forming NCOH (EQ30–DC46), and the NO-(H)CC isomer exhibits hydrogen atom elimination (EQ41–DC47).

Among the identified structures, the EQ0, EQ7, EQ9, EQ5, and EQ13 isomers are selected for reactivity analysis with H<sub>2</sub>O. These isomers serve as the initial fragment to react with H<sub>2</sub>O in potential product searching processes, performed at three

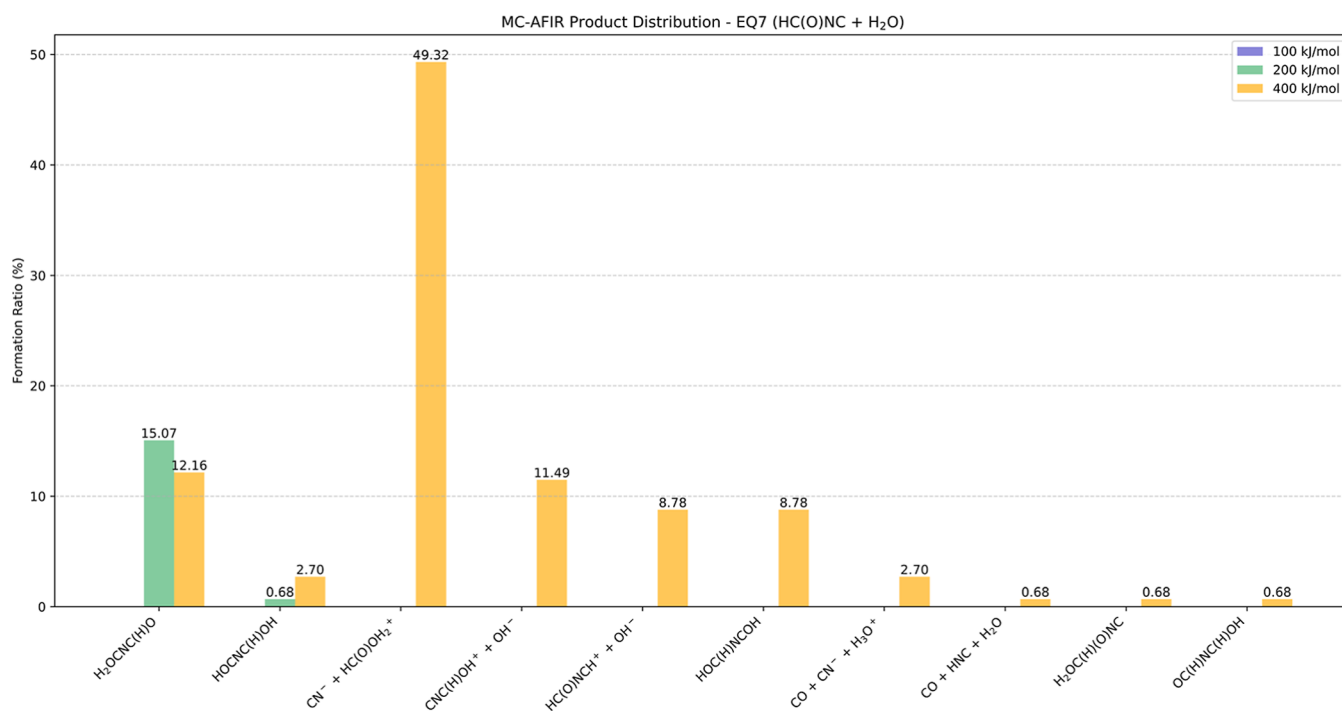


**Figure 4.** Predicted product distributions from MC-AFIR calculation for the reaction of HC(O)NC + H<sub>2</sub>O, starting from EQ7.

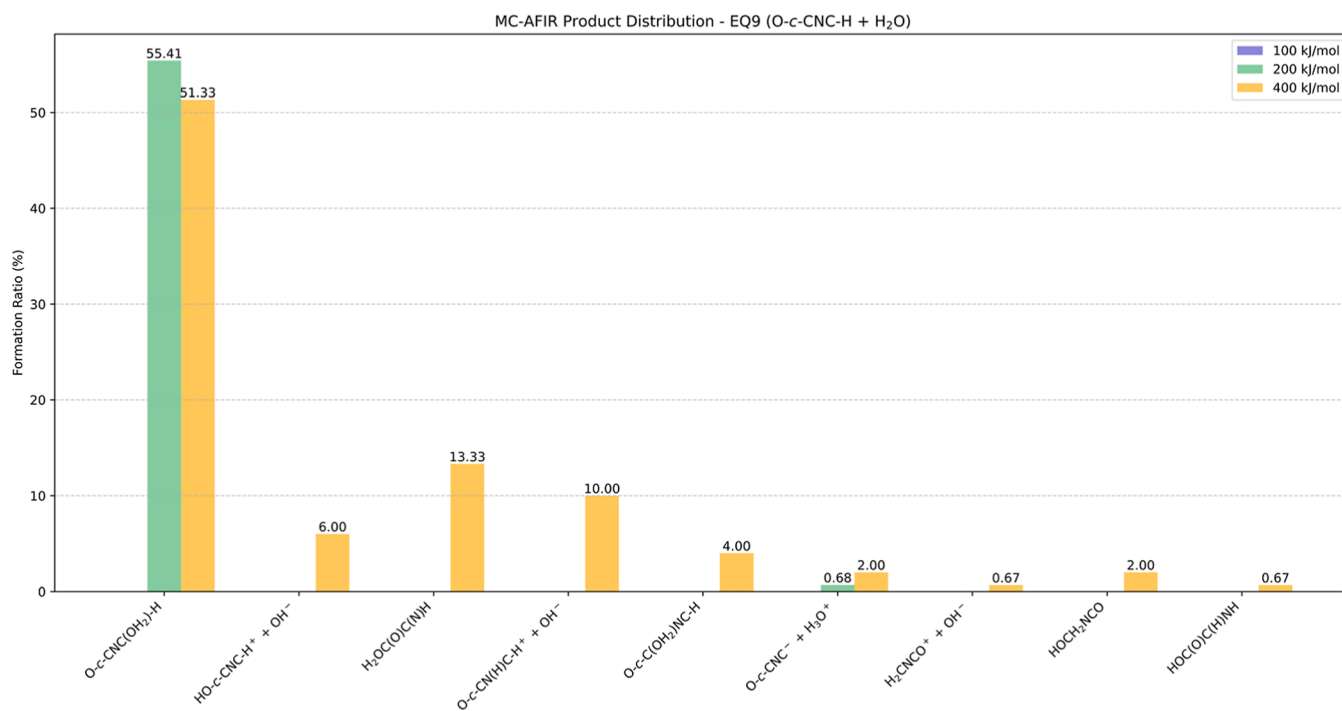


**Figure 5.** Predicted product distributions from MC-AFIR calculation for the reaction of O-c-CNC-H + H<sub>2</sub>O, starting from EQ9.

different  $\gamma$  values (100, 200, and 400 kJ/mol). The artificial forces facilitate the collision of isomers with a H<sub>2</sub>O molecule, generating structures that may serve as intermediates, products, or TS for subsequent reaction processes. Detailed information on MC-AFIR products is provided in the [Supporting Information](#).

The MC-AFIR calculations elucidate the distinct product distribution patterns in the reaction of EQ0 [HC(O)CN] and H<sub>2</sub>O across different artificial force constants (Table S5 and Figure 3). No product formation is observed at lower force

constants (100 and 200 kJ/mol), contrasted with significant reactivity emerges at 400 kJ/mol, suggesting a high activation barrier for this reaction. At  $\gamma = 400$  kJ/mol, the predominant product H<sub>2</sub>OC(H)(O)CN forms in 48.7% yield, while H<sub>2</sub>OC(N)C(O)H and the ionic species OH<sup>-</sup> + HOC(H)CN<sup>+</sup> are generated in yields of 11.5% and 10.1%, respectively, with additional minor products each comprising less than 7% of the total distribution. The product distribution indicates that molecular addition pathways for EQ0 and H<sub>2</sub>O are favored over ionic dissociation routes under these conditions.

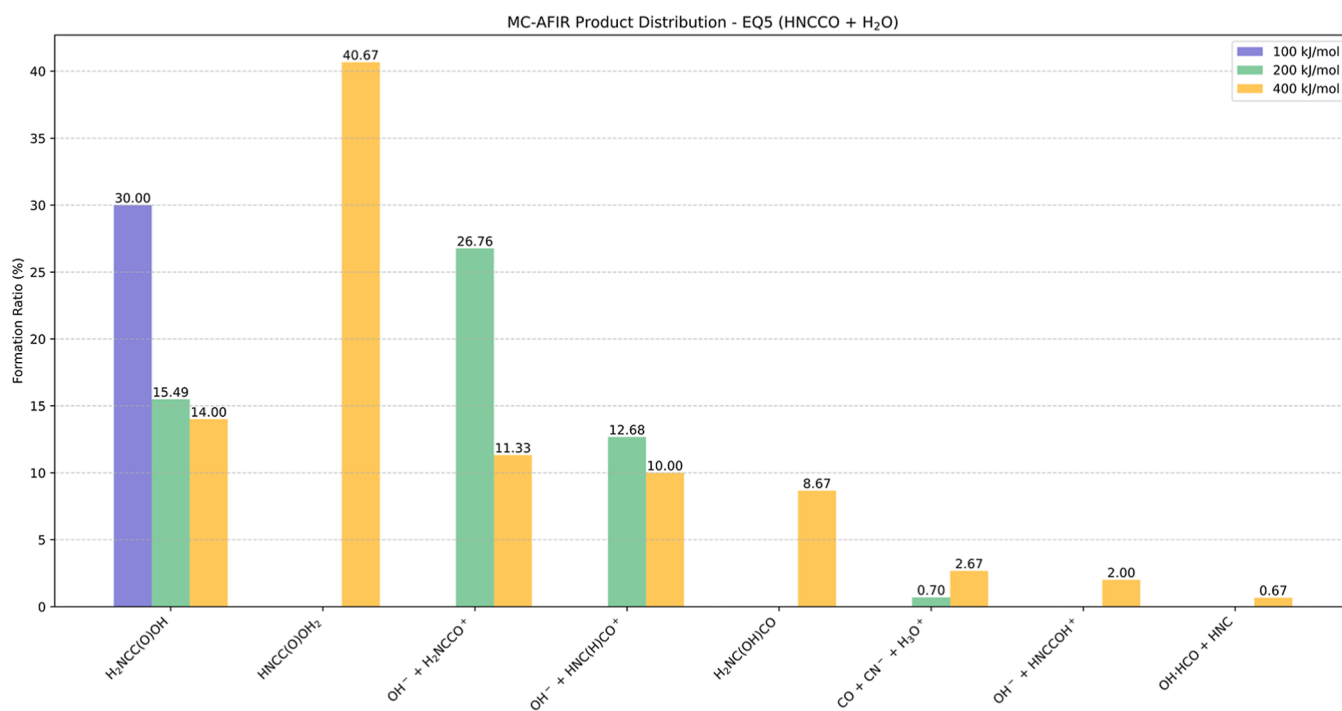


**Figure 6.** Predicted product distributions from MC-AFIR calculation for the reaction of HNCCO + H<sub>2</sub>O, starting from EQ5.

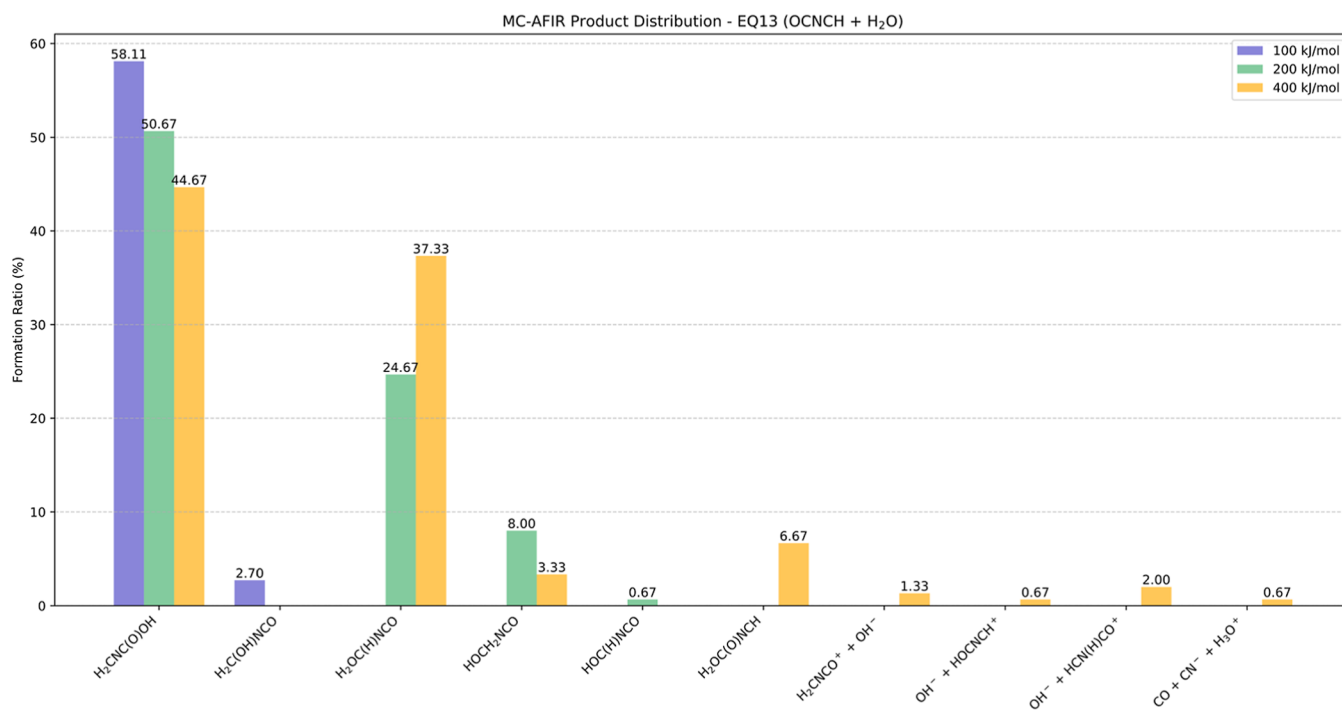


**Figure 7.** Predicted product distributions from MC-AFIR calculation for the reaction of OCNCH + H<sub>2</sub>O, starting from EQ13.

The reaction between EQ7 [HC(O)NC] and H<sub>2</sub>O is investigated with varying artificial force constants (Table S6 and Figure 4). At 100 kJ/mol, no reactivity is observed. However, product formation initiates at 200 kJ/mol, yielding predominately H<sub>2</sub>OCNC(H)O (15.1%) and trace amounts of HOCNC(H)OH (0.7%). Increasing the force constant to 400 kJ/mol results in a pronounced tendency toward ionization, characterized by the formation of CN<sup>-</sup> + HC(O)OH<sub>2</sub><sup>+</sup> ion pair as the major product (49.3%), accompanied by the formation of CNC(H)OH<sup>+</sup> + OH<sup>-</sup> (11.5%) and HC(O)-

NCH<sup>+</sup> + OH<sup>-</sup> (8.8%). Concurrently, the molecular addition product H<sub>2</sub>OCNC(H)O exhibits a slightly diminished yield (12.2%), while several minor products are observed at yields <3%. These product distributions indicate that elevated forces promote ionic dissociation pathways over molecular addition mechanisms in the EQ7–H<sub>2</sub>O system.

The MC-AFIR calculations elucidate the product distribution patterns for the reaction between EQ9 (O–*c*-CNC–H) and H<sub>2</sub>O under varying artificial force constants (Table S7 and Figure 5). At the lowest force constant (100 kJ/mol), no

product formation is observed. When increasing to 200 kJ/mol, the system shows increased reactivity, predominantly yielding the molecular addition product  $O-c-CNC(OH_2)-H$  (55.4%), with only trace amounts of  $O-c-CNC^- + H_3O^+$  (0.7%). At 400 kJ/mol, while  $O-c-CNC(OH_2)-H$  remains the major product (51.3%), several new products emerge through both molecular addition and ionic pathways. Notable products comprise  $H_2OC(O)C(N)H$  (13.3%) and the ionic pairs  $O-c-CN(H)C-H^+ + OH^-$  (10.0%) and  $HO-c-CNC-H^+ + OH^-$  (6.0%), with additional minor products forming in yields below 4%. These results suggest that for the EQ9– $H_2O$  system, molecular addition remains the preferred reaction pathway even with high activation energy, although ionic dissociation routes have become increasingly accessible.

The reactivity patterns between EQ5 (HNCCO) and  $H_2O$ , as revealed by MC-AFIR calculations (Table S8 and Figure 6), demonstrate unique force-dependent behavior. Notably, even at the lowest force constant (100 kJ/mol), the system exhibits reactivity with the exclusive formation of  $H_2NCC(O)OH$  (30.0%). As the force constant increases to 200 kJ/mol, the emergence of ionic species becomes prominent. The  $OH^- + H_2NCCO^+$  ion pair dominates (26.8%), followed by the formation of  $OH^- + HNC(H)CO^+$  (12.7%), while the initially observed  $H_2NCC(O)OH$  decreases to 15.5%. Further enhancement of the force constant to 400 kJ/mol triggers a significant mechanistic shift, with  $HNCC(O)OH_2$  emerging as the predominant product (40.7%). The original product  $H_2NCC(O)OH$  maintains a substantial presence (14.0%), while ionic pairs continue to form in significant quantities:  $OH^- + H_2NCCO^+$  (11.3%) and  $OH^- + HNC(H)CO^+$  (10.0%). Several additional products, including  $H_2NC(OH)-CO$  (8.7%) and various ionic species, form in minor quantities (less than 3%). This evolution in product distribution suggests a complex interplay between EQ5 and  $H_2O$ , with the preferred mechanism highly dependent on the activation energy.

MC-AFIR calculations reveal a distinct reactivity profile for the reaction between EQ13 (OCNCH) and  $H_2O$  (Table S9 and Figure 7). At  $\gamma = 100$  kJ/mol, the system already shows significant reactivity, predominantly forming  $H_2CNC(O)OH$  (58.1%) with a minor contribution of  $H_2C(OH)NCO$  (2.7%). When the force constant increases to 200 kJ/mol, while  $H_2CNC(O)OH$  remains the major product (50.7%), a new significant product  $H_2OC(H)NCO$  emerges (24.7%), along with  $HOCH_2NCO$  (8.0%) and trace amounts of  $HOC(H)-NCO$  (0.7%). At the highest force constant (400 kJ/mol), the system maintains its preference for molecular addition pathways, with  $H_2CNC(O)OH$  (44.7%) and  $H_2OC(H)NCO$  (37.3%) as the dominant products. Several new minor products appear, including  $H_2OC(O)NCH$  (6.7%) and  $HOCH_2NCO$  (3.3%), while small quantities of ionic species such as  $H_2CNCO^+ + OH^-$  (1.3%) and other ion pairs each form in yields below 2%. Notably, this reaction system demonstrates a consistent preference for molecular addition mechanisms across all force constants, with ionic pathways playing only a minor role even at higher forces.

## CONCLUSION

In this study, we conduct a comprehensive investigation of the PES of cyanoformaldehyde using the B3LYP-D3(BJ)/def2-TZVP level of theory, identifying a complex landscape of 48 EQs, 152 TSs, and 49 DCs. The global reaction route map reveals an intricate network comprising 80 distinct isomerization pathways, complemented by 34 TS-mediated and 40

direct DCs. Analysis of the investigated pathways reveals thermodynamic constraints on isomerization, with higher barriers generally protecting more stable isomers. Preliminary kinetic assessment demonstrates preferential transformation routes, though further dynamical studies including accurate tunneling correction are needed. Several pathways across the interstellar UV range (138.4–313.6 kcal/mol) indicate photochemically accessible transformations, but these isomers' thermodynamic instability would require continuous formation to maintain detectable concentrations. Through MC-AFIR calculations incorporating a single  $H_2O$  molecule, we elucidate the mechanistic influence of bimolecular interactions on product distribution. The systematic mapping of reaction pathways, combined with formation propensity analyses of water-involved products, provides fundamental insights into isomeric transformations and establishes a theoretical framework for predicting isomer distributions. Our findings demonstrate the utility of computational approaches in characterizing global reaction networks and offer valuable guidance for the selective detection and understanding of bimolecular reactions of cyanoformaldehyde isomers.

## ASSOCIATED CONTENT

### Supporting Information

The Supporting Information is available free of charge at <https://pubs.acs.org/doi/10.1021/acsomega.5c00949>.

Complete results of conformational investigations including Figures S1–S5 and Tables S1–S4; Cartesian coordinates for all EQ, TS, and DC structures from ADDF calculations; Global reaction route map (PDF)

## AUTHOR INFORMATION

### Corresponding Author

Naoki Kishimoto – Department of Chemistry, Graduate School of Science, Tohoku University, Sendai 980-8578, Japan; [orcid.org/0000-0003-2988-456X](https://orcid.org/0000-0003-2988-456X); Email: [kishimoto@tohoku.ac.jp](mailto:kishimoto@tohoku.ac.jp)

### Author

Dapeng Zhang – Department of Chemistry, Graduate School of Science, Tohoku University, Sendai 980-8578, Japan; [orcid.org/0000-0002-2879-5613](https://orcid.org/0000-0002-2879-5613)

Complete contact information is available at:

<https://pubs.acs.org/10.1021/acsomega.5c00949>

### Author Contributions

Conceptualization, investigation, formal analysis, visualization, and writing—original draft preparation, D.Z.; resources, project administration, and writing—review and editing, N.K. All authors have given approval to the final version of the manuscript.

### Notes

The authors declare no competing financial interest.

## ACKNOWLEDGMENTS

This work is supported by IQCE research funding and JSPS KAKENHI (Grants nos. 21K04806 and 24K08182) to N.K.

## REFERENCES

- (1) Lattelais, M.; Pauzat, F.; Ellinger, Y.; Ceccarelli, C. A New Weapon for the Interstellar Complex Organic Molecule Hunt: The Minimum Energy Principle. *Astron. Astrophys.* **2010**, *519*, A30.

- (2) Ellinger, Y.; Pauzat, F.; Markovits, A.; Allaire, A.; Guillemin, J.-C. The Quest of Chirality in the Interstellar Medium-I: Lessons of Propylene Oxide Detection. *Astron. Astrophys.* **2020**, *633*, A49.
- (3) Lattalais, M.; Pauzat, F.; Ellinger, Y.; Ceccarelli, C. Interstellar Complex Organic Molecules and the Minimum Energy Principle. *Astrophys. J.* **2009**, *696* (2), L133.
- (4) San Andrés, D.; Rivilla, V. M.; Colzi, L.; Jiménez-Serra, I.; Martín-Pintado, J.; Megías, A.; López-Gallifa, A.; Martínez-Henares, A.; Massalkhi, S.; Zeng, S.; et al. First Detection in Space of the High-energy Isomer of Cyanomethanimine: H<sub>2</sub>CNCN. *Astrophys. J.* **2024**, *967* (1), 39.
- (5) McGuire, B. A.; Shingledecker, C. N.; Willis, E. R.; Burkhardt, A. M.; El-Abd, S.; Motiyenko, R. A.; Brogan, C. L.; Hunter, T. R.; Margulés, L.; Guillemin, J.-C.; et al. ALMA Detection of Interstellar Methoxymethanol (CH<sub>3</sub>OCH<sub>2</sub>OH). *Astrophys. J., Lett.* **2017**, *851* (2), L46.
- (6) Hollis, J. M.; Lovas, F. J.; Jewell, P. R.; Coudert, L. H. Interstellar Antifreeze: Ethylene Glycol. *Astrophys. J.* **2002**, *571* (1), L59.
- (7) Ohno, K.; Satoh, H. Exploration on Quantum Chemical Potential Energy Surfaces: Towards the Discovery of New Chemistry. In *Theoretical and Computational Chemistry Series*; The Royal Society of Chemistry, 2022; Vol. 23, p 276. Chapter 1.
- (8) Lewis-Bevan, W.; Gaston, R. D.; Tyrrell, J.; Stork, W. D.; Salmon, G. L. Formyl Cyanide: A Stable Species. Experimental and Theoretical Studies. *J. Am. Chem. Soc.* **1992**, *114* (6), 1933–1938.
- (9) Bogey, M.; Destombes, J. L.; Vallee, Y.; Ripoll, J. L. Formyl Cyanide: Efficient Production from Allyloxyacetonitrile and Its Millimeter-Wave Spectrum. *Chem. Phys. Lett.* **1988**, *146*, 227–229.
- (10) Bogey, M.; Demuynck, C.; Destombes, J. L.; Vallee, Y. Millimeter-Wave Spectrum of Formyl Cyanide, HCOCN: Centrifugal Distortion and Hyperfine Structure Analysis. *J. Mol. Spectrosc.* **1995**, *172*, 344–351.
- (11) Judge, R. H.; Moule, D. C.; Biernacki, A.; Benkel, M.; Ross, J. M.; Rustenburg, J. Laser Excitation Spectrum and the Long Path Length Absorption Spectrum of Formyl Cyanide, CHOCN. *J. Mol. Spectrosc.* **1986**, *116*, 364–370.
- (12) Remijan, A. J.; Hollis, J. M.; Lovas, F. J.; Stork, W. D.; Jewell, P. R.; Meier, D. S. Detection of Interstellar Cyanoformaldehyde (CNCHO). *Astrophys. J., Lett.* **2008**, *675* (2), L85.
- (13) Gronowski, M.; Eluszkiewicz, P.; Custer, T. Structure and Spectroscopy of C<sub>2</sub>HNO Isomers. *J. Phys. Chem. A* **2017**, *121* (17), 3263–3273.
- (14) Fang, W.-H.; Liu, R.-Z.; You, X.-Z. Theoretical Study on Unimolecular Reactions of Formyl Cyanide. *Chem. Phys. Lett.* **1994**, *226*, 453–458.
- (15) Sengupta, D.; Peeters, J.; Nguyen, M. T. Theoretical Studies on C<sub>2</sub>H + NO Reactions: Mechanism for HCN + CO and HCO + CN Formation. *Chem. Phys. Lett.* **1998**, *283*, 91–96.
- (16) Chang, N.-Y.; Yu, C.-H. Ab Initio Study of the Dissociation of Formyl Cyanide. *Chem. Phys. Lett.* **1995**, *242*, 232–237.
- (17) Das, A.; Majumdar, L.; Chakrabarti, S. K.; Saha, R.; Chakrabarti, S. Formation of Cyanoformaldehyde in the Interstellar Space. *Mon. Not. R. Astron. Soc.* **2013**, *433* (4), 3152–3164.
- (18) Karpfen, A. On the Interaction of Cyanoformaldehyde with HNO, HF, HCl, H<sub>2</sub>O, and CH<sub>3</sub>OH: A Preference for Orthogonal Structures. *Comput. Theor. Chem.* **2017**, *1120*, 34–45.
- (19) Ohno, K.; Kishimoto, N.; Iwamoto, T.; Satoh, H. Global investigation of Isomers and Isomerization Channels on the Quantum Chemical Potential Energy Surface of H<sub>3</sub>CNO<sub>3</sub>. *J. Comput. Chem.* **2017**, *38* (7), 669–687.
- (20) Ohno, K.; Maeda, S. A Scaled Hypersphere Search Method for the Topography of Reaction Pathways on the Potential Energy Surface. *Chem. Phys. Lett.* **2004**, *384*, 277–282.
- (21) Ohno, K. Study of Potential Energy Surfaces towards Global Reaction Route Mapping. *Chem. Rec.* **2016**, *16* (5), 2198–2218.
- (22) Maeda, S.; Ohno, K. Global Mapping of Equilibrium and Transition Structures on Potential Energy Surfaces by the Scaled Hypersphere Search Method: Applications to ab Initio Surfaces of Formaldehyde and Propyne Molecules. *J. Phys. Chem. A* **2005**, *109* (25), 5742–5753.
- (23) Ohno, K.; Maeda, S. Global Reaction Route Mapping on Potential Energy Surfaces of Formaldehyde, Formic Acid, and Their Metal-Substituted Analogues. *J. Phys. Chem. A* **2006**, *110* (28), 8933–8941.
- (24) Maeda, S.; Ohno, K. A New Global Reaction Route Map on the Potential Energy Surface of H<sub>2</sub>CO with Unrestricted Level. *Chem. Phys. Lett.* **2008**, *460*, 55–58.
- (25) Ohno, K.; Maeda, S. Automated investigation of Reaction Channels. *Phys. Scr.* **2008**, *78*, 058122.
- (26) Maeda, S.; Harabuchi, Y.; Takagi, M.; Saita, K.; Suzuki, K.; Ichino, T.; Sumiya, Y.; Sugiyama, K.; Ono, Y. Implementation and Performance of the Artificial Force Induced Reaction Method in the GRRM17 Program. *J. Comput. Chem.* **2018**, *39* (4), 233–250.
- (27) Maeda, S.; Morokuma, K. A Systematic Method for Locating Transition Structures of A + B → X Type Reactions. *J. Chem. Phys.* **2010**, *132* (24), 241102.
- (28) Maeda, S.; Morokuma, K. Finding Reaction Pathways of Type A + B → X: Toward Systematic Prediction of Reaction Mechanisms. *J. Chem. Theory Comput.* **2011**, *7* (8), 2335–2345.
- (29) Maeda, S.; Harabuchi, Y.; Sumiya, Y.; Takagi, M.; Suzuki, K.; Hatanaka, M.; Osada, Y.; Taketsugu, T.; Morokuma, K.; Ohno, K. GRRM17, see [http://iqce.jp/GRRM/index\\_e.shtml](http://iqce.jp/GRRM/index_e.shtml) (accessed December 23, 2024).
- (30) Maeda, S.; Ohno, K.; Morokuma, K. Systematic investigation of the Mechanism of Chemical Reactions: The Global Reaction Route Mapping (GRRM) Strategy by the ADDF and AFIR Methods. *Phys. Chem. Chem. Phys.* **2013**, *15* (10), 3683–3701.
- (31) Frisch, M. J.; Trucks, G. W.; Schlegel, H. B.; Scuseria, G. E.; Robb, M. A.; Cheeseman, J. R.; Scalmani, G.; Barone, V.; Petersson, G. A.; Nakatsuji, H.; et al. *Gaussian 16*, Revision B.01; Gaussian, Inc., 2016.
- (32) Maeda, S.; Taketsugu, T.; Morokuma, K.; Ohno, K. Anharmonic Downward Distortion Following for Automated investigation of Quantum Chemical Potential Energy Surfaces. *Bull. Chem. Soc. Jpn.* **2014**, *87* (11), 1315–1334.
- (33) Grimme, S.; Antony, J.; Ehrlich, S.; Krieg, H. A Consistent and Accurate Ab Initio Parametrization of Density Functional Dispersion Correction (DFT-D) for the 94 Elements H-Pu. *J. Chem. Phys.* **2010**, *132* (15), 154104.
- (34) Grimme, S.; Ehrlich, S.; Goerigk, L. Effect of the Damping Function in Dispersion Corrected Density Functional Theory. *J. Comput. Chem.* **2011**, *32* (7), 1456–1465.
- (35) Weigend, F.; Ahlrichs, R. Balanced Basis Sets of Split Valence, Triple Zeta Valence and Quadruple Zeta Valence Quality for H to Rn: Design and Assessment of Accuracy. *Phys. Chem. Chem. Phys.* **2005**, *7* (18), 3297–3305.
- (36) Weigend, F. Accurate Coulomb-Fitting Basis Sets for H to Rn. *Phys. Chem. Chem. Phys.* **2006**, *8* (9), 1057–1065.
- (37) Chai, J. D.; Head-Gordon, M. Long-Range Corrected Hybrid Density Functionals with Damped Atom-Atom Dispersion Corrections. *Phys. Chem. Chem. Phys.* **2008**, *10* (44), 6615–6620.
- (38) Brémond, E.; Savarese, M.; Pérez-Jiménez, A.; Sancho-García, J. C.; Adamo, C. Range-Separated Double-Hybrid Functional from Nonempirical Constraints. *J. Chem. Theory Comput.* **2018**, *14* (8), 4052–4062.
- (39) Brémond, E.; Sancho-García, J. C.; Pérez-Jiménez, A.; Adamo, C. Communication: Double-Hybrid Functionals from Adiabatic-Connection: The QIDH Model. *J. Chem. Phys.* **2014**, *141* (3), 031101.
- (40) Møller, C.; Plesset, M. S. Note on an Approximation Treatment for Many-Electron Systems. *Phys. Rev.* **1934**, *46* (7), 618–622.
- (41) Dunning, T. H., Jr. Gaussian Basis Sets for Use in Correlated Molecular Calculations. I. The Atoms Boron Through Neon and Hydrogen. *J. Chem. Phys.* **1989**, *90* (2), 1007–1023.
- (42) Kendall, R. A.; Dunning, T. H., Jr.; Harrison, R. J. Electron Affinities of the First-Row Atoms Revisited. Systematic Basis Sets and Wave Functions. *J. Chem. Phys.* **1992**, *96* (9), 6796–6806.

(43) Raghavachari, K.; Trucks, G. W.; Pople, J. A.; Head-Gordon, M. A. Fifth-Order Perturbation Comparison of Electron Correlation Theories. *Chem. Phys. Lett.* **1989**, *157* (6), 479–483.

(44) Hollenbach, D. J.; Tielens, A. G. G. M. Dense Photo-dissociation Regions (PDRs). *Annu. Rev. Astron. Astrophys.* **1997**, *35* (1), 179–215.